

MIT Open Access Articles

*Tuning Areal Density and Surface Passivation
of ZnO Nanowire Array Enable Efficient PbS
QDs Solar Cells with Enhanced Current Density*

The MIT Faculty has made this article openly available. **Please share**
how this access benefits you. Your story matters.

Citation: Tavakoli Dastjerdi, Hadi, Prochowicz, Daniel, Yadav, Pankaj and Tavakoli, Mohammad Mahdi. 2019. "Tuning Areal Density and Surface Passivation of ZnO Nanowire Array Enable Efficient PbS QDs Solar Cells with Enhanced Current Density." *Advanced Materials Interfaces*, 7 (1).

As Published: <http://dx.doi.org/10.1002/admi.201901551>

Publisher: Wiley

Persistent URL: <https://hdl.handle.net/1721.1/140930>

Version: Author's final manuscript: final author's manuscript post peer review, without publisher's formatting or copy editing

Terms of Use: Article is made available in accordance with the publisher's policy and may be subject to US copyright law. Please refer to the publisher's site for terms of use.



Tuning Areal Density and Surface Passivation of ZnO Nanowire Array Enable Efficient PbS QDs Solar Cells with Enhanced Current Density

Hadi Tavakoli Dastjerdi,^{1} Daniel Prochowicz,² Pankaj Yadav,³ and Mohammad Mahdi Tavakoli^{4*}*

¹Department of Materials Science and Engineering, Massachusetts Institute of Technology, Cambridge, MA 02139, USA

²Institute of Physical Chemistry, Polish Academy of Sciences, Kasprzaka 44/52, 01-224 Warsaw, Poland

³Department of Solar Energy, School of Technology, Pandit Deendayal Petroleum University, Gandhinagar-382 007, Gujarat, India

⁴Department of Electrical Engineering and Computer Science, Massachusetts Institute of Technology, Cambridge, MA 02139, USA

E-mails: hadit@mit.edu, mtavakol@mit.edu

Keywords: colloidal quantum dots, lead sulfide, nanowire, photovoltaics, passivation

Abstract

Colloidal PbS quantum dots (QDs) have provoked a revolution in the field of optoelectronic devices owing to their low-cost fabrication processing and excellent physical properties. Recently, the fabrication of nanostructured PbS QDs photovoltaic (PV) devices based on zinc oxide (ZnO) nanowires array appeared as an effective strategy for improving the overall device performance. On

This is the author manuscript accepted for publication and has undergone full peer review but has not been through the copyediting, typesetting, pagination and proofreading process, which may lead to differences between this version and the [Version of Record](#). Please cite this article as [doi: 10.1002/admi.201901551](#).

This article is protected by copyright. All rights reserved.

the other hand, the infiltration of PbS QDs in a densely packed ZnO nanowire array not only impedes the efficient charge extraction but also increases the surface trap states and charge carrier recombination leading to degraded PV performance. Despite its potentially strong impact on the device performance, the role of nanowire areal density on photon absorption and exciton dynamics has not yet been studied and still remains unexplored. Here, for the first time, we tune the areal density of ZnO nanowires through controlling the precursor concentration and study its impact on PbS QDs PV performance. It is found that the device with optimized ZnO nanowire areal density yields significantly increased power conversion efficiency (PCE) (10.1% vs. 8.5% of control nanowire-based device) due to improved light scattering and reduced surface recombination states. To further improve the photovoltaic performance, we treated the ZnO nanowire surface with hydrogen plasma, which has not been studied before in QDs PVs. Transient photovoltage (TPV) measurement reveal that this passivation process noticeably reduces the nonradiative charge recombination yielding a champion device with a remarkable PCE of 10.8%.

1. Introduction

Colloidal quantum dots (CQDs) utilized for various optoelectronics devices [1-5] have attracted considerable attention as an emerging photovoltaic (PV) technology thanks to their tunable band gaps, high stability and solution processability [6-14]. Among them, lead sulfide (PbS) QDs devices [15-21] are particularly interesting due to their stability in air and size-tunable bandgaps with certified reported PCE up to 12% [22]. However, in these device structures, the optimum thickness of PbS QDs layer for absorbing all of the incoming photons is larger than the carrier diffusion length, leading to reduced carrier collection. In order to enhance the light absorption and carrier diffusion length

without compromising collection efficiency, the interface engineering approaches such as utilization of functional organic ligands to passivate the surface states of QDs [23, 24] or dot-to-dot surface coupled self passivation schemes have been extensively studied [25]. However, the diffusion length still falls short of the optimum thickness for efficiently harvesting all near-infrared photons [26]. As an alternative approach, the ordered bulk heterojunction (OBHJ) architectures such as ZnO nanowires embedded within PbS QDs PV structure have been utilized to decouple the direction of photon absorption and charge collection [27-32]. This method allows to use thick QDs active layer and greatly improves the charge extraction and short-circuit current (J_{SC}). Employing ZnO nanowires within PbS QDs PV has resulted in remarkably high J_{SC} values of 31 mA/cm² and PCE of 9.6% [30]. Moreover, very recently, record-high J_{SC} values exceeding 33 mA/cm² with PCEs of 10.6% have been demonstrated for PbS QDs PV with embedded ZnO nanowires utilizing a luminescence down-shifting strategy [31]. Despite the increased value of J_{SC} , the reported highly dense ZnO nanowire arrays imposes some limitations on the device performance. This mostly stems from the presence of large densities of surface states due to the large surface-to-volume ratio of ZnO nanowires, which is detrimental to PV performance. In addition, closely packed ZnO nanowire arrays decreases the interfacial area between the absorber layer and nanowires leading to impeded carrier extraction. Thus, the ZnO nanowires should be sufficiently “wet” with QDs to reduce the path that the photogenerated carriers need to travel before they are extracted. Moreover, the light scattering and thereby optical absorption property of the QDs devices with densely packed ZnO nanowire arrays need improvement to enhance optical absorption inside the device structure. Despite its strong impact on the performance of QDs PVs, the role of nanowire areal density still remains to be studied. It is also expected that the high density of surface states of ZnO nanowires adversely impact the photovoltaic performance of such devices. Therefore, surface passivation strategies that help to reduce the density of ZnO nanowire surface states are expected to enhance the charge carrier collection and overall PV

performance of PbS QDs devices. The photoluminescence (PL) studies of ZnO nanowires have commonly revealed the presence of green emission, in addition to the main near band emission, which is mostly attributed to the presence of nanowire surface states [32]. Therefore, different surface treatments such as AlO_x coating [33], Ar ion milling [34] and polymer covering [35] have been performed to suppress this deep level emission. Recently, hydrogen plasma (H-plasma) treatment was used to enhance the ZnO optical property by effectively quenching the green emission peak [36].

Here, for the first time, we demonstrate that by tailoring the areal density of grown ZnO nanowires and thereby the density of nanowire surface states and optical transmittance, the carrier collection and overall performance of PbS QDs devices are improved. Also they could benefit other PV devices such as polymer [37] and perovskite solar cells [38-40]. In this work, we use the precursor concentration as a handle to tailor the ZnO nanowire growth, which results in PCE increase from 8.5% for the device with highest ZnO nanowire areal density to 10% for the optimal ZnO nanowire areal density. Further passivation of ZnO nanowires using hydrogen plasma (H-plasma) successfully suppresses the non-radiative recombination leading to devices with a maximum PCE of 10.8%.

2. Results and Discussion

Figure 1a and **1b** show the schematic illustration of the PbS QDs device structure and energy band alignment of the ITO, ZnO/ZnO nanowire, PbS-TBAI and PbS-EDT layers at equilibrium. A 40 nm thick textured polycrystalline seed film of ZnO was initially deposited on pre-patterned ITO substrates by a sol-gel process (for details see the Experimental Section). The ZnO nanowires were grown on the ZnO seed layer at 90 °C for 40 min using solution containing equal volume of zinc nitrate hexahydrate and hexamethylenetetramine in DI water (25 mL). The concentrations of precursor solution used for ZnO nanowire growth were selected to be 0.05 M, 0.033 M, 0.016 M and 0.008 M,

which we further refer to as A, B, C and D, respectively. For reference, a planar sample with only ZnO seed layer was also prepared. Next, PbS QDs with the first absorption peak at ~ 950 nm in solution (Figure. 1c) were deposited using a layer-by-layer deposition method. To replace the native oleic acid ligands in the first 10 layers, a solution of tetrabutylammonium iodide (TBAI) in methanol was used. The ligand exchange for the last 2 layers was performed by using a solution of 1,2-ethanedithiol (EDT) in acetonitrile. Au electrode was deposited by thermal evaporation through a shadow mask. The focused ion beam (FIB)-milled scanning electron microscopy (SEM) image of the PbS QDs/ZnO nanowire device is shown in Figure. 1d.

The scanning electron microscopy (SEM) images of the ZnO nanowire arrays grown with different concentrations show that the nanowire areal density is reduced by decreasing the concentration (**Figure 2a**). Figure 2b and 2c demonstrate the changes of height and diameter of ZnO nanowires and nanowire density with respect to precursor concentration, respectively. It is found that either nanowire dimension and length decrease with reducing the concentration. However, the decreased in the nanowire diameter is more pronounced, reducing from ~ 30 nm for sample A to ~ 23 nm for sample D. These results are consistent with the previously reported studies on ZnO nanowires growth at different concentrations [41, 42].

The PV metrics and current density-voltage (J - V) characteristics of planar reference and PbS QDs/ZnO nanowire devices were measured under 100 mW cm^{-2} simulated AM 1.5MG illumination and are shown in **Figure 3a**, Figure 3b and Table S1 in the Supporting Information. The planar reference device shows the highest V_{oc} in compared to all ZnO nanowire based PbS QDs devices. The V_{oc} drops by about 7% for the device with the highest ZnO nanowire areal density (device A). As expected, the resulting PbS QDs/ZnO nanowire devices show noticeable increase in J_{sc} in comparison

to planar reference device. The highest improvement in J_{sc} was observed for the device B and device C, which resulted in 27% and 30% PCE improvement compared to planar reference device, respectively. The improvement in V_{oc} of devices C and D (low concentration) can be attributed to the decreased areal density of ZnO nanowires, which considerably reduces the total number of nanowire surface states that would otherwise act as non-radiative recombination centers (vide infra). The champion device C yielded a V_{oc} of 595 mV and PCE of 10.1% under 100 mW cm^{-2} AM1.5G illumination.

The comparison of the semi-log dark J - V characteristics of representative planar and ZnO nanowire PbS QDs devices shows that device A exhibits higher current leakage (Figure S2, Supporting Information) which can be attributed to the significantly enhanced carrier recombination at the heterointerface. To further evaluate the carrier recombination in PbS QDs/ZnO nanowire devices, we studied the variations of their V_{oc} as a function of light intensity and extracted their diode ideality factors (n). For PV devices with significant trap-assisted charge recombination, the value of n is larger than 1 ($1 < n < 2$) [43] and PbS QDs devices usually have ideality factor in the range of 1.5-2 [44-46]. The light-intensity dependence of the V_{oc} was studied according to the relation $V_{oc} \propto \frac{n k T}{q}$ where n is the diode ideality factor, T is the temperature, k is the Boltzmann constant and q is elementary charge [16, 47]. Fitting the V_{oc} vs. light intensity of resulting PbS QDs devices yielded the values of n as 1.3, 1.9 and 1.45, for the planar device, device A and device C, respectively (Figure 3c). The value of n for the devices B and D are determined to be 1.76 and 1.35, respectively as shown in Figure S3. Since the only difference between these devices is the degree of areal density of incorporated ZnO nanowires, these results strongly suggest that the trap-assisted charge

recombination at the ZnO nanowire/QDs interface was monotonically suppressed by reducing the areal density of ZnO nanowires.

As mentioned above, the J_{SC} of the ZnO nanowire based PbS QDs devices is noticeably higher than that of planar device due to improved charge collection. External quantum efficiency (EQE) spectra were measured to further confirm the obtained photocurrent values and shown in Figure 3d. The corresponding integrated photocurrent densities were also calculated by integrating the AM1.5G spectrum with the EQE spectra. The J_{SC} values obtained from the J - V curves are $\sim 1 \text{ mA/cm}^2$ higher than those of the calculated J_{SC} from EQE results. This difference is due to the spectral mismatch between the spectra of the utilized solar simulator and that of AMG 1.5. The enhancement in J_{SC} for PbS QDs devices with ZnO nanowires grown at lower concentration (devices C and D) can be attributed to the increased optical transmittance and improved light scattering. However, the value of J_{SC} for device D is similar to that of device A (high concentration) likely due to the presence of small ZnO nanowires areal density of this sample to effectively contribute in photo-generated carrier collection.

Figure 4a shows the transmittance spectra of the investigated ZnO nanowires films deposited on ITO/glass substrates. We note that all ZnO nanowire-based films show higher transmittance compared to planar reference film. As previously reported in the literature [48], nanowires work as an antireflection layer due to their optical scattering effect (out-coupling property), which can increase the transmittance and decrease the reflectance of ITO glass substrate as compared to planar ZnO. For light management in the nanostructures, one of the main parameters for nanowire array is their pitch size, defined as the distance between the cores of two adjacent nanowires. In order to effectively reduce the reflectance of nanowire array, the optimum value for pitch size is

required. Previously, we studied the role of pitch size in a nanocone array (as an anti-reflection layer) on the reflectance spectra and device performance. Our FDTD simulation results and reflectance measurement in that study revealed that 1 micrometer pitch size is the best condition for reducing the reflection in the device [49]. Moreover, in the literature, many people studied the role of pitch size on optical properties of nanowire arrays [50, 51]. For example, Hua et al. [50] found that by controlling the diameter of nanowire and the pitch size, they can drastically enhance the absorption of germanium (Ge) nanowire arrays (reduce its reflection), as they proved it by FDTD simulation as well. They found that 500 nm pitch size with 300 nm diameter for Ge nanowires show the best absorption (lowest reflection). Similar principle can be applied to our ZnO nanowire array study. By decreasing the areal density to ~ 150 (per μm^2) for sample C, we will have a lowest reflection, due to the light scattering effect. We have included the measured reflectance spectra of different nanowire samples in Fig. S4, Supporting Information. In the absence of optical absorption for ZnO at wavelengths > 400 nm, the difference in transmittance of different nanowires is due to their different reflectance spectra, for instance, the lower transmittance of the nanowire sample with the highest areal density is due to its higher reflectance. The transmittances of films B and C are higher than that of film A, which well-corroborate with their corresponding J_{SC} values. Moreover, the transmittance for film D is lower than that found in other ZnO nanowire-based devices suggesting reduced optical absorption, which in fact can be a reason for its lower J_{SC} . The reduced areal density of the ZnO nanowires grown at lower concentration could potentially facilitate their infiltration with PbS QDs. In order to gain more information about carrier recombination inside the device structure, we employed electrochemical impedance spectroscopy (EIS) [52, 53] (for the discussion and data see

Figure S5 in the Supporting Information), which confirms the reduction of exciton recombination for the devices with lower areal density of ZnO nanowires.

The hydrogen plasma treatment (see experimental section) was performed on sample with optimal precursor concentration (device C) to passivate ZnO nanowire surface states and further improve the photovoltaic performance. Figure 4b shows the room-temperature PL spectra of the as-prepared and H-plasma treated ZnO nanowires films. Both spectra exhibit the near band emission of ZnO at around 380 nm together with a significantly broader emission in the visible region. The PL spectrum of the H-plasma treated ZnO nanowire shows a clear enhancement of the near band emission accompanied with a significant quenching of the visible emission peak. The enhancement of the near band emission can be attributed to the reduced nonradiative recombination centers as a result of ZnO nanowire surface passivation [54]. Recent work revealed that increase of radiative recombination can be a result of H doping [55] and might be also partially played a role here too.

X-ray electron spectroscopy (XPS) was performed to study the composition of ZnO nanowire surface before and after H-plasma treatment. The O 1s peak of the ZnO nanowire samples before and after H-passivation are shown in Figure 4c. Deconvolution of the spectra shows two main peaks located at 529.9 and 531.3 eV, which are attributed to Zn-O-Zn and hydroxyl groups, respectively [35, 56, 57]. In contrast to the Zn-O-Zn peak, which is similar in intensity for both samples, the H-plasma treated film shows a noticeable increase of the hydroxyl group peak. This result suggests that H-plasma treatment passivated O- dangling bonds on the ZnO nanowire surface and thereby reduced the density of surface states.

Figure 5a shows the representative J - V characteristics of the optimized PbS QDs devices with and without H-plasma treatment. Compared with the non-treated device with a PCE of 9.9%, the H-plasma passivated device shows improvement in PV metrics leading to a maximum PCE of 10.8%. The EQE spectra of the devices and integrated current densities confirm the photocurrent improvement upon H-plasma treatment (Figure 5b). We believe that the small reverse saturation current together with the reduced charge recombination upon ZnO nanowire surface passivation are likely the reasons for improved values of V_{oc} and FF. The light-intensity dependence of the V_{oc} was measured for passivated and unpassivated devices, as shown in Figure 5c. The n value for the passivated device is extracted to be ~ 1.33 , which is noticeably lower than that of the unpassivated device ($n = 1.45$) suggesting a reduced trap-assisted charge recombination. To confirm this result, we analyzed the devices using the transient photovoltage (TPV) measurements (at open-circuit condition with 1 sun light bias) (Figure 5d). The device with passivated ZnO nanowires exhibits a clearly slower voltage decay (1005 μ s) compared to unpassivated device (830 μ s), which further confirms the reduced density of trap states for the passivated device. In addition, the electroluminescence (EL) measurements at $V = 1$ (V) show stronger emission peak for the passivated device, which is likely due to decreased non-radiative recombination centers at the nanowire/QDs interface (Figure 6a). The passivation process also reduces the reverse leakage current (Figure 6b) and recombination resistance indicating a lower charge recombination at the PbS QDs/ZnO nanowire interface (Figure 6c). The devices with and without passivation show good stability after storing in ambient environment over 7 days (Figure S6, Supporting Information).

3. Conclusion

In summary, the impact of areal density of ZnO nanowires as an ETL inside PbS QDs PV was studied and a direct correlation between nanowire density and PV performance was observed. The areal density of ZnO nanowires was precisely optimized by controlling the precursor concentration, resulting in enhanced optical transmittance of ZnO ETL. We found that areal density of $\sim 150 \mu\text{m}^{-2}$ (corresponding to nanowire growth precursor concentration of 0.016 M) has the best effect on the absorption and device performance leading to a champion device with a high J_{SC} of 30 mA/cm^2 and PCE of 10.1%. To further improve the device performance, the surface of ZnO nanowires was treated by H-plasma. We demonstrated that this process significantly reduces the nanowire surface states leading to a device with improved PCE up to 10.8%. Our results demonstrate that the precise control of ZnO nanowire growth together with H-plasma treatment can be utilized to manipulate the optical and electrical characteristics, and as a result improve the overall PV performance. The proposed ZnO nanowire growth and H-plasma passivation processes are not only limited to PbS QDs PV and could also benefit other PV devices such as polymer and perovskites solar cells.

4. Experimental Section

PbS QDs Device Fabrication and plasma treatment: After cleaning ITO substrates of 200 nm thickness in DI water and acetone, the substrates were exposed to oxygen plasma (PDC 32G, Harrick Plasma) for 1 min. A solution of zinc acetate dihydrate (0.3 M) and ethanolamine (0.3 M) in 2-methoxyethanol was spincoated on the cleaned ITO substrates followed by an annealing step (200°C for 15 min). PbS colloidal QDs with native oleic acid ligands and first exciton absorption peak in solution positioned at $\sim 950 \text{ nm}$ were synthesized as previously reported in literature [58, 59]. Layer by layer PbS QDs deposition onto the ZnO-coated ITO/glass substrates was performed by spincoating. A solution of PbS QDs with concentration of 50 mg/mL in octane was spincoated at 2000 rpm for 25 s. TBAI (Sigma-Aldrich) exchange for the native oleic acid capping ligands was performed using a TBAI solution in methanol with 10 mg/mL concentration and waiting 25 s

followed by spin-drying, and two times rinsing with methanol. The QDs deposition steps with TBAI ligand exchange were repeated for 10 layers. The ligand exchange for the last 2 layers was done using a solution of 1,2-ethanedithiol (EDT) in acetonitrile, waiting 25 s followed by spin-drying, and two times rinsing with acetonitrile. The concentration of EDT solution was 0.02 vol% in acetonitrile. All spincoating steps were carried out under ambient conditions. Au electrodes (Kurt J. Lesker, 99.999%) were deposited by thermal evaporation through a shadow mask -deposition rate of 1 Å/sec- at a base pressure of 10^{-6} Torr. The solar cell area of the device with Au electrode was measured to be 0.054 cm². The hydrogen-plasma treatment was performed with a dc plasma for 20 min at room temperature. The plasma power was set at 20 W and the pressure was set at 15 mTorr.

Device Characterization: Current–voltage (J – V) characteristics were measured in a nitrogen-filled glovebox by a semiconductor device analyzer (Agilent Technologies, B1500A). The solar simulator illumination of 100 mWcm⁻² was provided by a 150 W xenon arc-lamp (Newport 96000) with an AM1.5G filter. Optical transmittance and absorbance spectra were measured by a UV-VIS/NIR spectrometer (Lambda 1050). EQE was measured by a 250 (W) tungsten halogen lamp source with an Oriel Cornerstone 130 monochromator. Integrated photocurrent densities were calculated by integrating the product of the EQE and the AM1.5G spectra over the wavelength range of 370–1100 nm. PL spectra were measured with a SpectraPro 300i spectrometer equipped with liquid nitrogen cooled InGaAs detector arrays (Princeton Instruments). EL spectra were collected on the same setup as for the PL measurements using a 2400 Keithley sourcemeter. XPS measurements were performed using an X-ray photoelectron spectrometer (ESCALAB 250Xi, Thermo Fisher SCIENTIFIC INC., USA) with Al K α radiation ($h\nu = 1486.6$ eV) as a source. The transient photovoltage decay measurements were done with a Tektronix TDS 3054B oscilloscope using a pulse laser light source emitting at 532 nm under white light bias provided by solar simulator. A series of neutral density filters were used between the light source and the device for light intensity dependence measurements. The SEM imaging was performed using a FEI Helios NanoLab 600 at 5 kV. To prepare device cross-sections for SEM, Ga focused ion beam (FIB) milling at 30 kV was used on the same tool.

Supporting Information

Supporting Information is available from the Wiley Online Library or from the author.

Acknowledgements

This work was in part supported by Natural Sciences and Engineering Research Council (NSERC) of Canada (Award number: PDF-487850-2016). D.P. acknowledges the financial support from the HOMING program of the Foundation for Polish Science co-financed by the European Union under the European Regional Development Fund (POIR.04.04.00-00-5EE7/18-00). M.M.T. would like to acknowledge research laboratory of electronics (RLE) at Massachusetts institute of technology.

Received: ((will be filled in by the editorial staff))

Revised: ((will be filled in by the editorial staff))

Published online: ((will be filled in by the editorial staff))

References

- [1] J. Gao, A. F. Fidler, V. I. Klimov, *Nat. Commun.* **2015**, *6*, 8185.
- [2] G. Konstantatos, I. Howard, A. Fischer, S. Hoogland, J. Clifford, E. Klem, L. Levina, E. H. Sargent, *Nature* **2006**, *442*, 180.
- [3] A. F. Fidler, J. Gao, V. I. Klimov, *Nat. Phys.* **2017**, *13*, 604.
- [4] Z. Ren, J. Sun, H. Li, P. Mao, Y. Wei, X. Zhong, J. Hu, Sh. Yang, J. Wang, *Adv. Mater.* **2017**, *29*, 1702055.
- [5] Y. Shirasaki, G. J. Supran, M. G. Bawendi, V. Bulović, *Nat. Photonics* **2013**, *7*, 13-23.
- [6] M. Yuan, M. Liu, E. H. Sargent, *Nat. Energy* **2016**, *1*, 16016.
- [7] M. L. Böhm, T. C. Jellicoe, M. Tabachnyk, N. J. L. K. Davis, F. Wisnivesky-Rocca-Rivarola, C. Ducati, B. Ehrler, A. A. Bakulin, N. C. Greenham, *Nano lett.* **2015**, *15*, 7987-7993.
- [8] H. Aqoma, S.-Y. Jang, *Energy Environ. Sci.* **2018**, *11*, 1603-1609.
- [9] G. H. Carey, A. L. Abdelhady, Z. Ning, S. M. Thon, O. M. Bakr, E. H. Sargent, *Chem. Rev.* **2015**, *115*, 12732-12763.
- [10] M. V. Kovalenko, *Nat. Nanotechnol.* **2015**, *10*, 994.

- [11] A. Swarnkar, A. R. Marshall, E. M. Sanehira, B. D. Chernomordik, D. T. Moore, J. A. Christians, T. Chakrabarti, J. M. Luther, *Science* **2016**, *354*, 92.
- [12] J. Yuan, X. Ling, D. Yang, F. Li, S. Zhou, J. Shi, Y. Qian, J. Hu, Y. Sun, Y. Yang, X. Gao, S. Duhm, Q. Zhang, W. Ma, *Joule* **2018**, *2*, 2450.
- [13] X. Ling, S. Zhou, J. Yuan, J. Shi, Y. Qian, B. W. Larson, Q. Zhao, C. Qin, F. Li, G. Shi, C. Stewart, J. Hu, X. Zhang, J. M. Luther, S. Duhm, W. Ma, *Adv. Energy Mater.* **2019**, *9*, 1900721.
- [14] F. Li, S. Zhou, J. Yuan, C. Qin, Y. Yang, J. Shi, X. Ling, Y. Li, W. Ma, *ACS Energy Lett.* **2019**, *4*, 2571-2578.
- [15] M. Liu, O. Voznyy, R. Sabatini, F. P. García de Arquer, R. Munir, A. H. Balawi, X. Lan, F. Fan, G. Walters, A. R. Kirmani, S. Hoogland, F. Laquai, A. Amassian, E. H. Sargent, *Nat. Mater.* **2017**, *16*, 258.
- [16] H. T. Dastjerdi, R. Tavakoli, P. Yadav, D. Prochowicz, M. Saliba, M. M. Tavakoli, *ACS Appl. Mater. Interfaces* **2019**, *11*, 26047-26052.
- [17] W. Xu, F. Tan, Q. Liu, X. Liu, Q. Jiang, L. Wei, W. Zhang, Z. Wang, Sh. Qu, Z. Wang, *Sol. Energy Mater. Sol. Cells* **2017**, *159*, 503-509.
- [18] X. Lan, O. Voznyy, F. P. García de Arquer, M. Liu, J. Xu, A. H. Proppe, G. Walters, F. Fan, H. Tan, M. Liu, Zh. Yang, S. Hoogland, E. H. Sargent, *Nano lett.* **2016**, *16*, 4630-4634.
- [19] K. Lu, Y. Wang, Z. Liu, L. Han, G. Shi, H. Fang, J. Chen, X. Ye, S. Chen, F. Yang, A. G. Shulga, T. Wu, M. Gu, S. Zhou, J. Fan, M. A. Loi, W. Ma, *Adv. Mater.* **2018**, *30*, 1707572.
- [20] M. M. Tavakoli, A. Simchi, Z. Fan, H. Aashuri, *ChemComm.* **2016**, *52*, 323-326.
- [21] M. M. Tavakoli, H. Aashuri, A. Simchi, Z. Fan, *Phys. Chem. Chem. Phys.* **2015**, *17*, 24412-24419.
- [22] J. Xu, O. Voznyy, M. Liu, A. R. Kirmani, G. Walters, R. Munir, M. Abdelsamie, A. H. Proppe, A. Sarkar, F. P. Garcia de Arquer, M. Wei, B. Sun, M. Liu, O. Ouellette, R. Quintero - Bermudez, J. Li, J. Fan, L. Quan, P. Todorovic, H. Tan, S. Hoogland, S. O. Kelley, M. Stefiik, A. Amassian, E. H. Sargent, *Nat. Nanotechnol.* **2018**, *13*, 456.
- [23] Y. Cao, A. Stavrinadis, T. Lasanta, D. So, G. Konstantatos, *Nat. Energy* **2016**, *1*, 16035.
- [24] C. H. Chuang, P. R. Brown, V. Bulović, M. G. Bawendi, *Nat. Mater.* **2014**, *13*, 796-801.
- [25] G. H. Carey, L. Levina, R. Comin, O. Voznyy, E. H. Sargent, *Adv. Mater.* **2015**, *27*, 3325-3330.

- [26] D. Zhitomirsky, O. Voznyy, S. Hoogland, E. H. Sargent, *ACS Nano* **2013**, 7, 5282-5290.
- [27] H. Wang, V. Gonzalez-Pedro, T. Kubo, F. Fabregat-Santiago, J. Bisquert, Y. Sanehira, J. Nakazaki, H. Segawa, *J. Phys. Chem. C* **2015**, 119, 27265-27274.
- [28] H. Wang, T. Kubo, J. Nakazaki, H. Segawa, *ACS Energy Lett.* **2017**, 2, 2110-2117.
- [29] T. Kawawaki, H. Wang, T. Kubo, K. Saito, J. Nakazaki, H. Segawa, T. Tatsuma, *ACS Nano* **2015**, 9, 4165-4172.
- [30] P. H. Rekemeyer, S. Chang, C. -H. M. Chuang, G. W. Hwang, M. G. Bawendi, S. Gradecak, *Adv. Energy Mater.* **2016**, 6, 24.
- [31] H. T. Dastjerdi, D. Prochowicz, P. Yadav, M. M. Tavakoli, *Sustainable Energy Fuels* **2019**, 3, 3128-3134.
- [32] I. Shalish, H. Temkin, V. Narayanamurti, *Phys. Rev. B* **2004**, 69, 245401.
- [33] J. Richters, T. Voss, D. Kim, R. Scholz, M. Zacharias, *Nanotechnology* **2008**, 19, 305202.
- [34] R. Chen, Q.-L. Ye, T. He, T. Wu, H. Sun, *Appl. Phys. Lett.* **2011**, 98, 241916.
- [35] K. Liu, R. Chen, G. Xing, T. Wu, H. Sun, *Appl. Phys. Lett.* **2010**, 96, 023111.
- [36] Y. Li, M. Zhong, T. Tokizono, I. Yamada, G. Bremond, J.-J. Delaunay, *Nanotechnology* **2011**, 22, 435703.
- [37] M. M. Tavakoli, H. T. Dastjerdi, J. Zhao, K. E. Shulenberger, C. Carbonera, R. Po, A. Cominetti, G. Bianchi, N. D. Klein, M. G. Bawendi, S. Gradecak, J. Kong, *Small* **2019**, 15, 1900508.
- [38] D. - Y. Son, J. - H. Im, H. - S. Kim, N. - G. Park, *J. Phys. Chem. C* **2014**, 118, 16567.
- [39] N. Islavath, G. Lingamallu, *Sol. Energy* **2018**, 170, 158-163.
- [40] A. Dymshits, L. Iagher, L. Etgar, *Materials* **2016**, 9, 60.
- [41] G. Amin, M. Asif, A. Zainelabdin, S. Zaman, O. Nur, M. Willander, *J. Nanomater.* **2011**, 2011, 5.
- [42] M. Guo, P. Diao, S. Cai, *J. Solid State Chem.* **2005**, 178, 1864-1873.
- [43] Y. Zhang, G. Wu, C. Ding, F. Liu, Y. Yao, Y. Zhou, C. WuNaoki, N. Qingxun, H. Taro Toyoda, R. Wang, Sh. Hayase, Z. Zou, Q. Shen, *J. Phys. Chem. Lett.* **2018**, 9, 3598-3603.
- [44] M. J. Speirs, D. M. Balazs, H.-H. Fang, L.-H. Lai, L. Protesescu, M. V. Kovalenko, M. A. Loi, *J. Mater. Chem. A* **2015**, 3, 1450-1457.
- [45] S. Pradhan, A. Stavrinadis, S. Gupta, Y. Bi, F. Di Stasio, G. Konstantatos, *Small* **2017**, 13, 1700598.
- [46] Z. Jin, A. Wang, Q. Zhou, Y. Wang, J. Wang, *Sci. Rep.* **2016**, 6, 37106.

- [47] M. J. Speirs, D. N. Dirin, M. Abdu-Aguye, D. M. Balazs, M. V. Kovalenko, M. A. Loi, *Energy Environ. Sci.* **2016**, *9*, 2916-2924.
- [48] J. V. S. Krishna, G. Reddy, K. Devulapally, N. Islavath, L. Giribabu, *Opt. Mater.* **2019**, *95*, 109243.
- [49] M. M. Tavakoli, K.-H. Tsui, S.-F. Leung, Q. Zhang, J. He, Y. Yao, D. Li, Z. Fan, *ACS Nano* **2015**, *9*, 10287.
- [50] B. Hua, B. Wang, M. Yu, P. W. Leu, Z. Fan, *Nano Energy* **2013**, *2*, 951.
- [51] S. F. Leung, Q. Zhang, M. M. Tavakoli, J. He, X. Mo, Z. Fan, *Small* **2016**, *12*, 2536.
- [52] H. Wang, Y. Wang, B. He, W. Li, M. Sulaman, J. Xu, Sh. Yang, Y. Tang, B. Zou, *ACS Appl. Mater. Interfaces* **2016**, *8*, 18526-18533.
- [53] A. K. Rath, T. Lasanta, M. Bernechea, S. L. Diedenhofen, G. Konstantatos, *Appl. Phys. Lett.* **2014**, *104*, 063504.
- [54] W. Kim, G. Kwak, M. Jung, S. K. Jo, J. B. Miller, A. J. Gellman, K. Yong, *J. Phys. Chem. C* **2012**, *116*, 16093-16097.
- [55] A. Dev, R. Niepelt, J. Richters, C. Ronning, T. Voss, *Nanotechnology* **2010**, *21*, 065709.
- [56] H. K. Yadav, K. Sreenivas, V. Gupta, S. Singh, R. Katiyar, *J. Mater. Res.* **2007**, *22*, 2404-2409.
- [57] M. Chen, X. Wang, Y. H. Yu, Z. L. Pei, X. D. Bai, C. Sun, R. F. Huang, L.S. Wen, *Appl. Surf. Sci.* **2000**, *158*, 134-140.
- [58] M. A. Hines, G. D. Scholes, *Adv. Mater.* **2003**, *15*, 1844-1849.
- [59] Ni Zhao, T. P. Osedach, L. Chang, S. M. Geyer, D. Wanger, M. T. Binda, A. C. Arango, M. G. Bawendi, V. Bulovic, *ACS Nano* **2010**, *4*, 3743-3752.

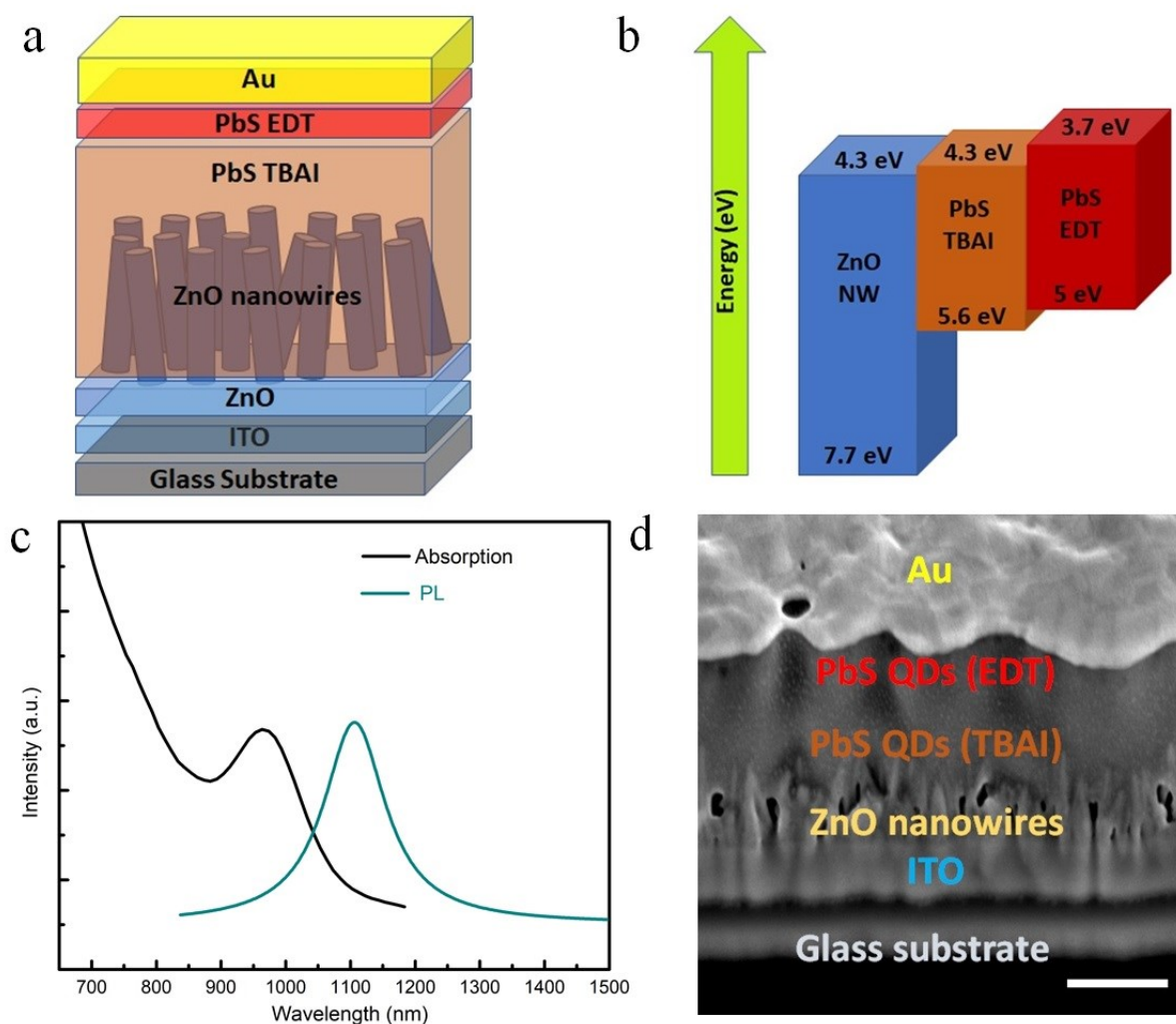


Figure 1. a) Schematic illustration of the PbS QDs PV device structure. b) Schematic qualitatively demonstrating the band alignment of the ZnO/ZnO nanowire, PbS-TBAI, and PbS-EDT layers at equilibrium, with typical conduction and valence band energy levels relative to vacuum as measured using ultraviolet photoelectron spectroscopy (UPS) and reported elsewhere [24, 30] c) Absorption and PL spectra of PbS QDs. d) FIB-milled cross section SEM image of PbS QDs PV. Scale bar is 200 nm.

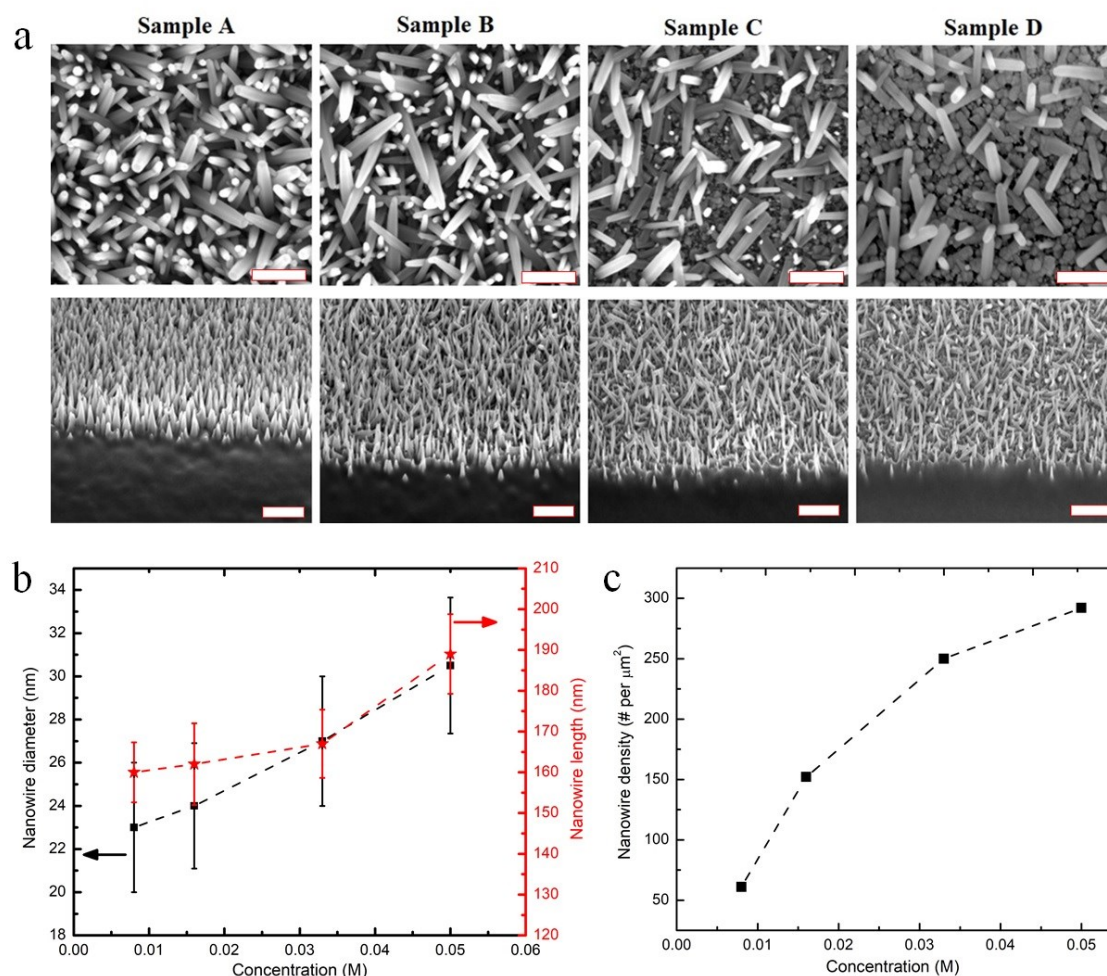


Figure 2. a) SEM images of ZnO nanowire arrays grown with different precursor concentration resulting in different nanowire areal densities. b) Structural dimensions of nanowires grown at different precursor concentrations. c) Areal densities for nanowires grown at different precursor concentrations. The areal density (number of nanowires per μm^2) for each nanowire sample was calculated by counting the number of nanowires in randomly chosen square-shaped areas of $0.5 \mu\text{m} \times 0.5 \mu\text{m}$ in their corresponding top view SEM image. Five images for each condition were considered from which the average value of areal density was calculated. Scale bar is 100 nm.

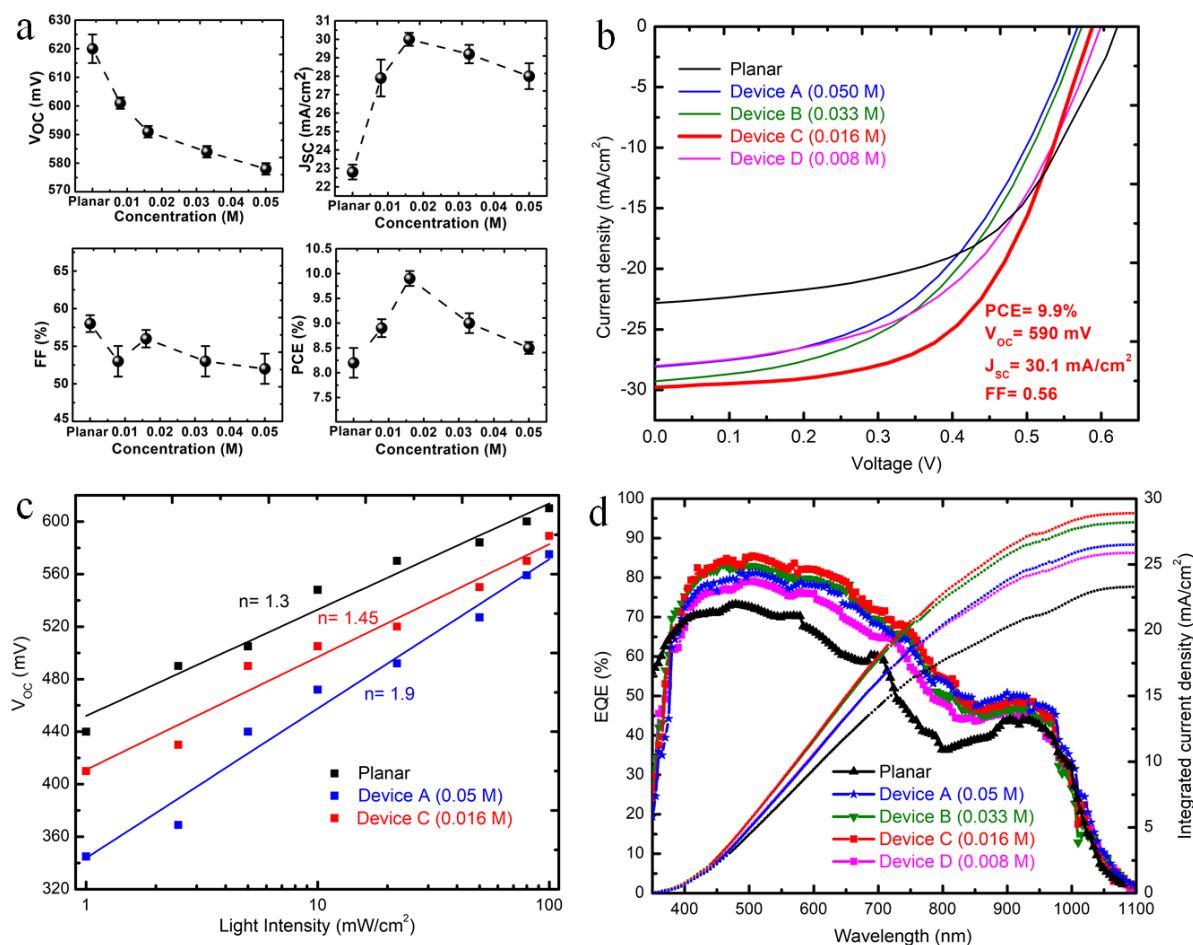


Figure 3. a) Device performance metrics for planar and ZnO nanowire-based PbS QDs devices under 100 mW cm⁻² AM1.5G illumination. Each data point represents six devices for each sample (details shown in Table S1, Supporting Information). b) J-V characteristics of representative planar and ZnO nanowire-based devices grown with different precursor concentrations. c) V_{oc} of PbS QDs PV embedding nanowires of different areal densities as a function of light intensity. d) EQE spectra for planar and nanowire devices grown with different precursor concentrations and their calculated corresponding integrated photocurrents.

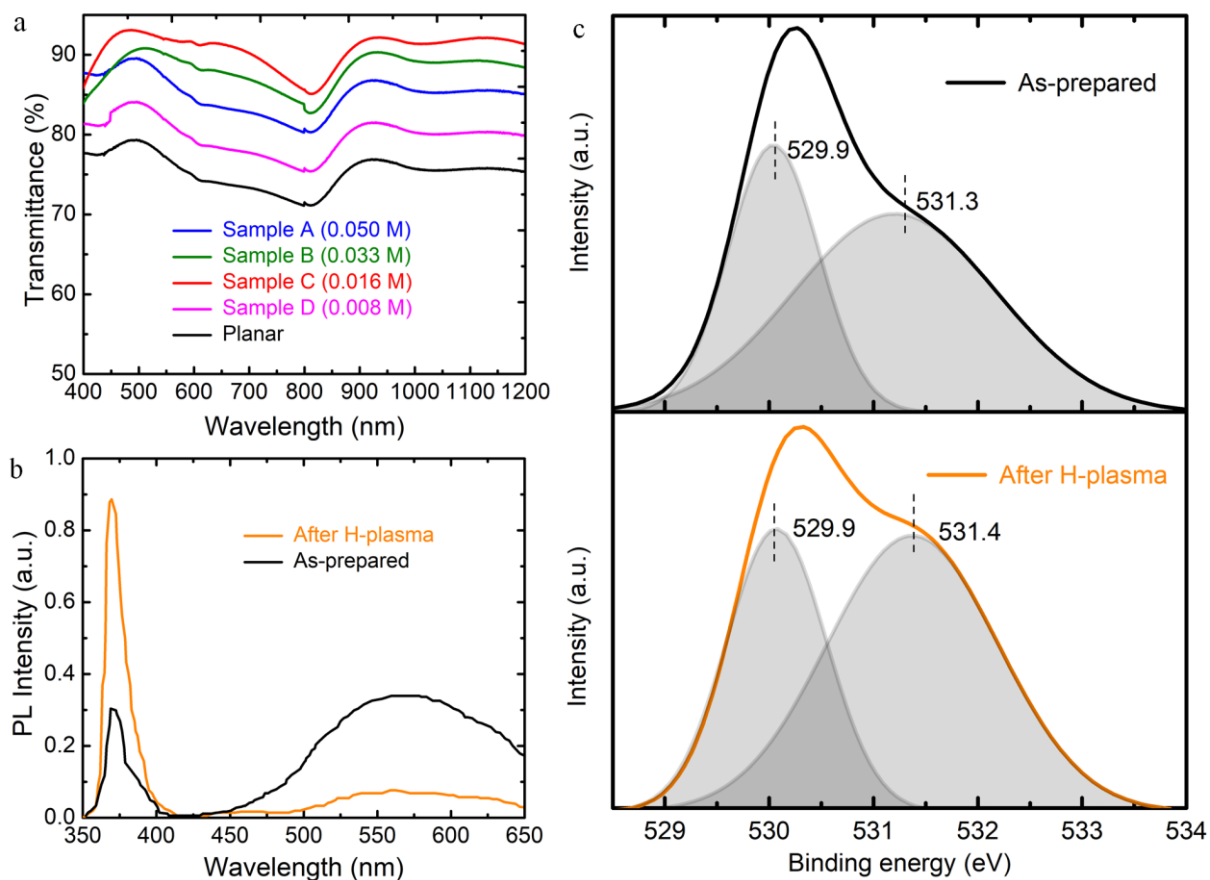


Figure 4. a) Transmittance spectra of ZnO nanowires with different areal densities and grown on ITO/glass substrates. The planar structure consists of only ZnO seed layer on similar ITO/glass substrate. b) Room-temperature PL spectra of the as-grown and H plasma-treated ZnO nanowires. c) XPS spectra of O 1s peaks of as-grown and H-plasma treated nanowires showing increase in the intensity of hydroxyl group peak after H-plasma treatment.

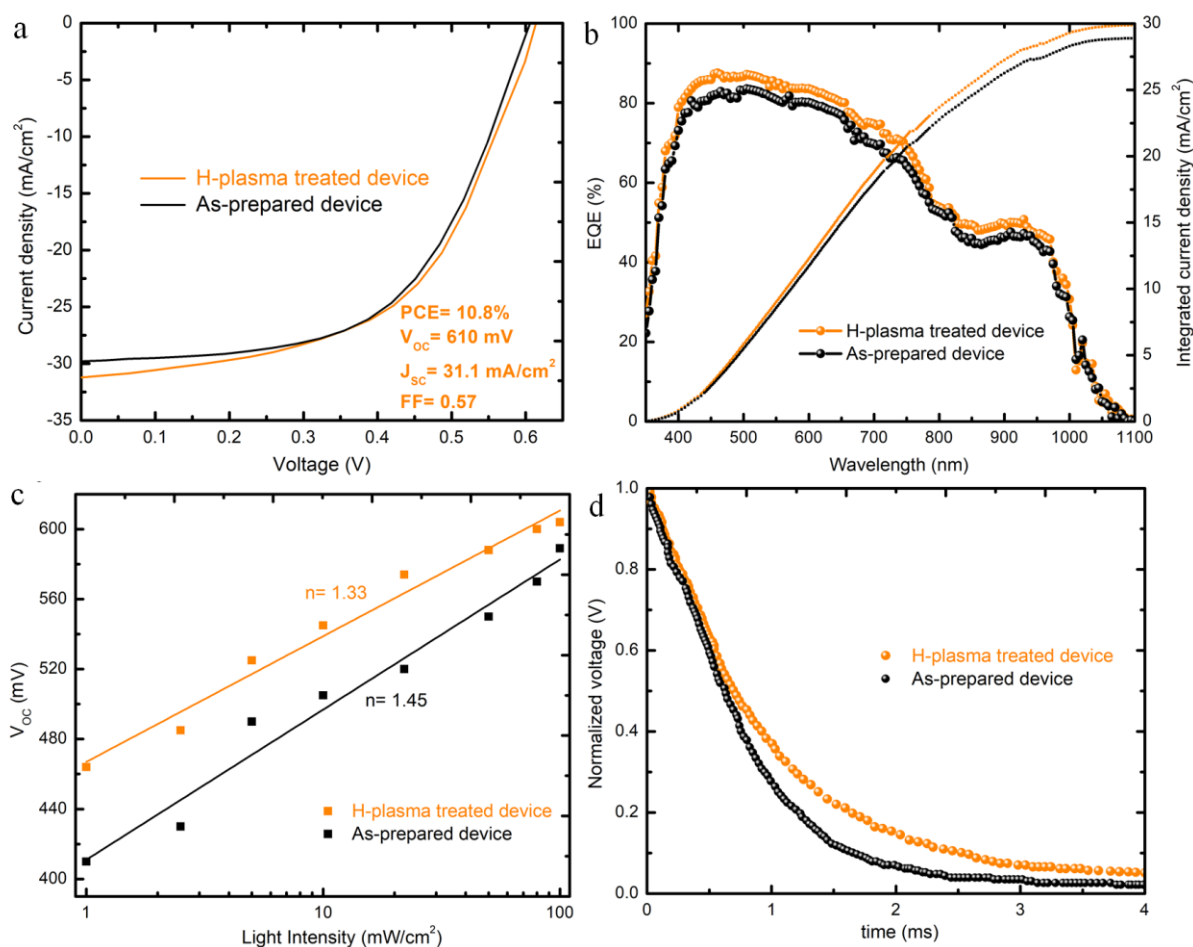


Figure 5. a) J - V characteristics of optimized as-prepared and after H-plasma treated PbS QDs/ZnO nanowire devices measured under 100 mW cm^{-2} AM1.5G illumination. PV characteristics of six devices on each sample are presented in Table S1, Supporting Information. b) EQE spectra of optimized as-prepared and after H-plasma treated PbS QDs/ZnO nanowire devices and their corresponding integrated photocurrents c) V_{oc} as a function of light intensity for optimized as-prepared and after H-plasma treated PbS QDs/ZnO nanowire devices. d) Transient photovoltage decay measurements of optimized as-prepared and after H-plasma treated PbS QDs/ZnO nanowire devices.

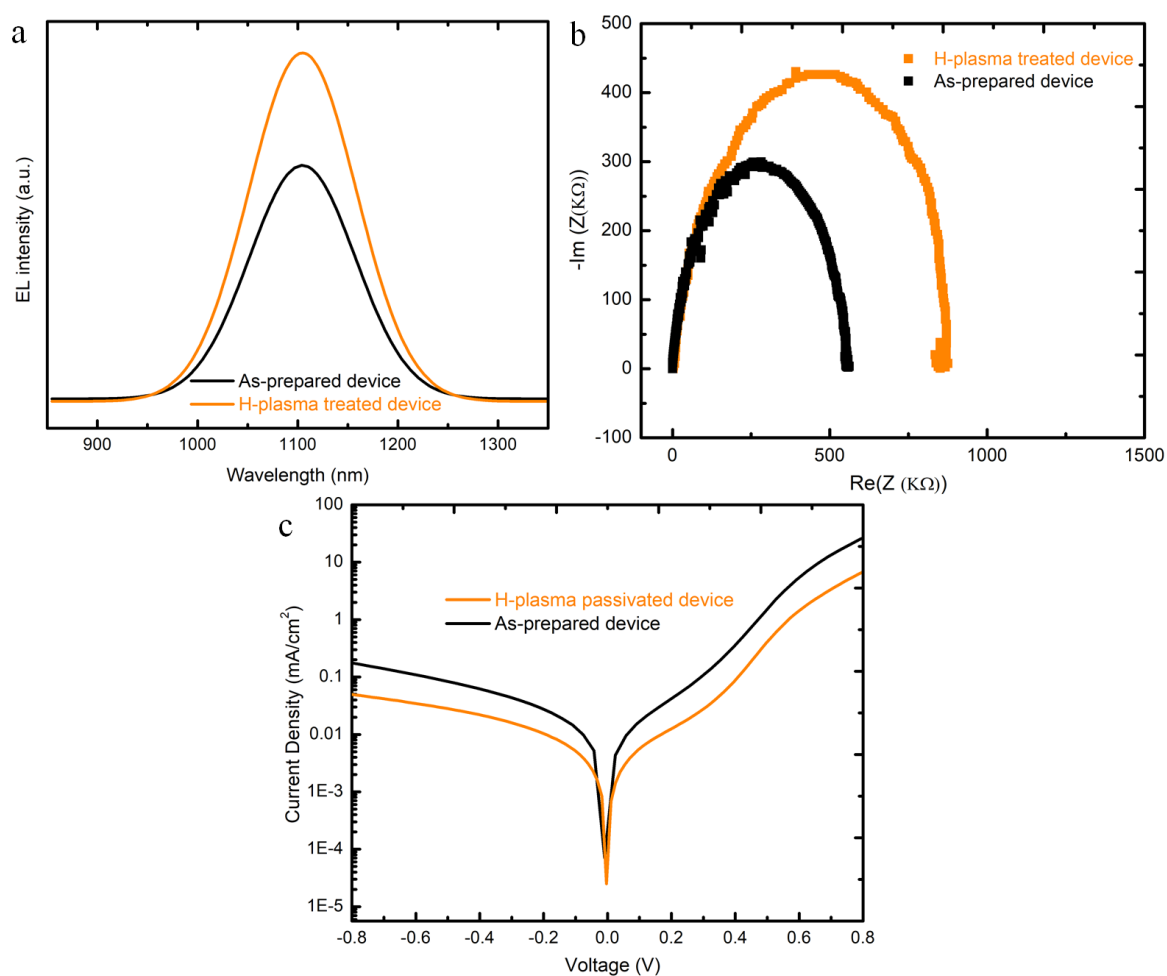


Figure 6. a) EL spectra of PbS QDs/nanowire PV embedding passivated and unpassivated nanowires showing improved EL for passivated device indicative of reduced nonradiative recombination. b) Semi-log dark J - V characteristics of representative passivated and unpassivated devices of optimal nanowire areal density showing reduced leakage current for the passivated device. c) Cole-Cole plots of impedance spectroscopy measurements under 0 (V) bias at dark condition for passivated and unpassivated devices showing increased recombination resistance upon nanowire surface passivation.

Remarkably enhanced PV performance for PbS quantum dot PVs is achieved through tuning the areal density of ZnO nanowire arrays, due to noticeably improved optical absorption and

significant reduction of nonradiative recombination. Furthermore, surface passivation of ZnO nanowire array by hydrogen plasma results in improved PCE from 10.1% to 10.8%.

colloidal quantum dots, lead sulfide, nanowire, photovoltaics, passivation

Hadi Tavakoli Dastjerdi,* Daniel Prochowicz, Pankaj Yadav, and Mohammad Mahdi Tavakoli*

Tuning Areal Density and Surface Passivation of ZnO Nanowire Array Enable Efficient PbS QDs Solar Cells with Enhanced Current Density

